YBa_2Cu_3O_X高温超伝導セラミクスの臨界電流密度の改善に関する実験的研究

鄭, 旭光
九州大学工学研究科電子工学専攻

https://doi.org/10.11501/3054174

出版情報：九州大学, 1990, 工学博士, 課程博士
バージョン：
権利関係：

AN EXPERIMENTAL APPROACH TO IMPROVEMENT OF CRITICAL CURRENT DENSITY IN HIGH-T_c $YBa_2Cu_3O_x$ CERAMICS

XUGUANG ZHENG

AN EXPERIMENTAL APPROACH TO IMPROVEMENT OF CRITICAL CURRENT DENSITY IN HIGH-T_c $YBa_2Cu_3O_x$ CERAMICS

XUGUANG ZHENG

KYUSHU UNIVERSITY

FACULTY OF ENGINEERING

DEPARTMENT OF ELECTRONICS

JANUARY, 1991

CONTENTS

1. INTRODUCTION

1.1. Superconductivity and its applications

When electrical current flows through a metal, part of the electrical energy is lost as Joul heat because any metal has an electrical resistance. Generally, the resistance decreases when the ambient temperature is lowered. A residual resistance resulting from impurities and defects, remains even if the metal is cooled down to 0 K.

However, in some metals, the resistance falls to zero at a well-defined temperature. This striking phenomenon is called superconductivity and the temperature at which a material transforms from its normal state to the superconducting state is called the transition temperature, T_c. Superconductivity was first discovered in mercury by Kamerlingh-Onnes in 1911.[1)] Since then it has been discovered in many metals, alloys and even oxides.

In a ring made of the superconducting material, the closed current set up in it will flow permanently without any decay. This is an obvious consequence of the zero resistance.

The superconducting material is able to transmit power without any transmission loss or to generate strong magnetic field by winding into a many-turns coil.

In an ordinary magnet made of copper wires, large amount of power is consumed to maintain the magnetic field. It turns to Joul heat and accumulates in the magnet. As the result a great quantity of water is used to cool the magnet. Because of this reason, the obtainable magnetic field with an ordinary magnet is also limited. As a matter of fact, very strong magnetic fields (> 10 Tesla) are usually obtained with magnets made from superconducting materials.

In itself, the vanishing of the resistance has not yet lead to a good understanding of the phenomenon of superconductivity. In fact, in a perfect conductor, i.e. an ideal metal without any impurities or defects, the resistance can be regarded as zero. The important discovery, in this respect, is the so-called Meissner effect, discovered by Meissner and Ochsenfeld in 1933.[2] This effect shows the difference of behaviour between a perfect conductor and a superconductor, in the presence of a magnetic field.

Figure 1.1 shows the variation of the magnetic induction in the interior of a long solid cylinder of a superconductor when the applied field H is parallel to the axis of the cylinder. When the field is increased from zero to a certain field H_c, surface currents suppress the penetration of the field and the induction B is zero in the interior of the sample. Up to now the superconductor behaves exactly like a perfect conductor.

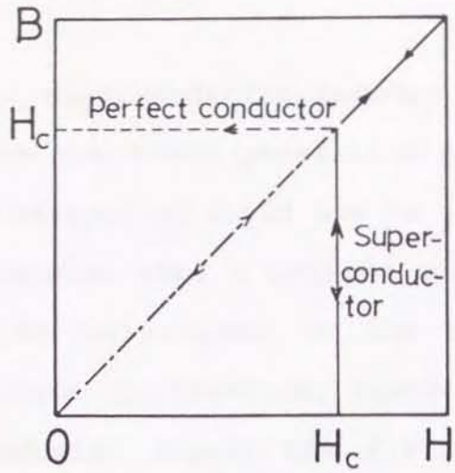

Fig. 1.1. Variation of the induction versus field for a superconductor and a perfect conductor.

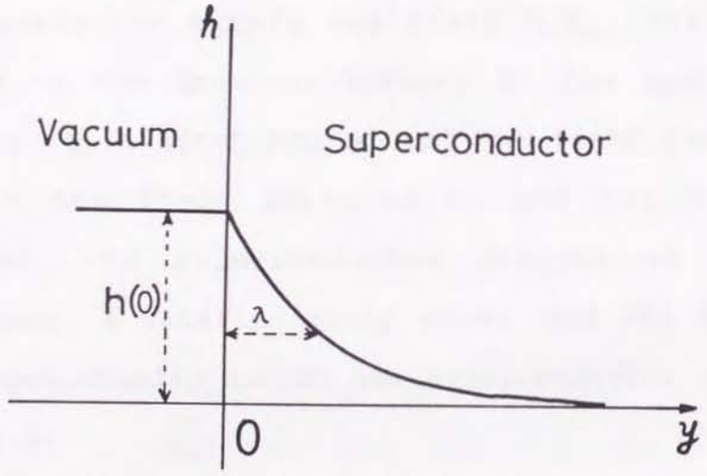

Fig. 1.2. Penetration of the field inside a superconductor.

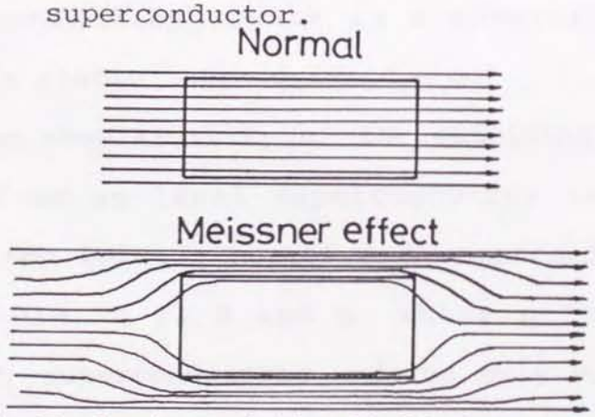

Fig. 1.3. Exclusion of the field from a superconductor (Meissner effect).

At $H=H_c$ the superconductor becomes a normal conductor and therefore the field penetrates and B becomes equal to H_c. Let the applied field now be lowered below H_c. If the superconductor were a perfect conductor, the induction would be maintained to the value $B=H_c$ by the surface currents. In practice, however, it is found that the superconductor expels the field and that B=0 for $0<H<H_c$.

Thus, at a given temperature $T<T_c$, an ideal superconductor expels any field $H<H_c$. This does not depend on the previous history of the specimen, i.e. whether it is first cooled and the field then switched on, or the field switched on and the temperature reduced. The superconductor behaves as a perfect diamagnet. A detailed study shows that the field falls off exponentially inside the superconductor as shown in Fig. 1.2.

The Meissner effect proves that the "superconducting" state is a reversible equilibrium state, a stable thermodynamic one.

The reversibility of the expulsion of a magnetic field from an ideal superconductor implies that the transition between normal and superconducting state is reversible in T, H and p, where p is the pressure. However, superconductors undergo only very small volume changes and the pressure dependence can be neglected. Thus the two phases are separated by a threshold curve

$H=H_c(T)$. $H_c(T)$ has approximately a parabolic variation with T, i.e.

$$H_c(T)=H_c(0)[1-T^2/T_c^2]. \qquad (1.1)$$

For $T>T_c$ the material is normal even in zero field.

Utilizing the superconducting property, there are many technical applications as follows.

Superconducting wires can be used for power transmission. Because of the zero resistance, it is able to transport and distribute large blocks of power efficiently at a low cost.

Superconducting coil can act as magnet. It can be used in thermonuclear fusion research, NMR and medical science etc.. It is also expected to bring revolutionary changes to transportation by introduction of the so-called linear motorcar and superconducting electro-magnetic thrust ship.

Besides, superconductor can be used in motors, generators, computer devices, magnetometers and many other specific applications. Applying superconductivity, great progresses in energy, transportation, information, medicine and a lot of specific fields of science and technology can be achieved.

1.2. History of superconductors

Superconductivity had long been regarded as a phenomenon belonging to the low temperature physics. In fact, until 1986, the transition temperature T_c had remained below 25 K with an enhancing rate of $\sim$0.3 K per year in spite of continuous efforts.

Because of the low T_c, liquid helium must be used to cool the superconductors in practical uses. As widely known, helium is a rare resources in limited areas and the cost is very high. Therefore, the practical applications are largely limited.

One important question arises. Are higher T_cs available? And how does the superconductivity occur?

Bardeen, Cooper and Schrieffer (BCS) gave a theoretical explanation for the superconducting phenomenon in 1957.[3] An abstract can be made as follows. Superconductivity occurs when electrons of Fermi particles are coupled into pairs (Cooper pair) which are Bose particles. In a solid state material, this pairing is realized by the intermediation of lattice vibration (phonons). The displaced ions induced by one electron attracts the other electron. However, this coupling is destroyed at temperature T_c at which the random thermal movement of ions increases to an extent large enough to destroy the ordered lattice vibration.

According to the BCS theory, the transition temperature T_c can be expressed as

$$T_c \sim \Theta_D \exp[-1/N(0)V]. \qquad (1.2)$$

Where Θ_D is Debye temperature which corresponds to the average energy of phonons. N(0) is the state density of electrons in Fermi surface, and V can be viewed as the attraction force between the two electrons in a Cooper pair.

With higher Θ_D, N(0) and V, higher T_c could be obtained. However, these three parameters are correlated to each other. Thus it is difficult to raise them at the same time. According to the BCS theory, the upper limit of T_c exists at $\sim\Theta_D/10 \doteq 30\text{-}40$ K.

All kinds of superconductors had been explained successfully by the BCS theory and the upper limit of T_c had been never broken. However, a revolutionary breakthrough came in 1986. First, Bednorz and Muller reported a T_c of 30 K in a La-Ba-Cu-O compound.[4] Since then surprising high T_cs have been achieved in many other oxide compounds, bringing a brand new age to the modern science and technology. Within only three years, the critical temperature T_c has been rocketed to a value as high as 120 K.[5] These high T_cs clearly exceed the predicted limit in the BCS theory. Other mechanism of the electrical carrier coupling are explored widely.

All of the newly discovered high-T_c superconductors have similar structures being characterized by a Cu-O based perovskite type. Among them, $YBa_2Cu_3O_x$ is a representative one which has very steady superconducting state below 90 K.[6] Because of the high T_c, areas of application are greatly extended. The merit of such a high T_c is that the superconducting state can be obtained by liquid nitrogen cooling. Unlike helium, nitrogen can be easily separated from the air at a much lower cost.

In Fig. 1.4, history of the T_c increase is illustrated. In Fig. 1.5, the perovskite structured $YBa_2Cu_3O_x$ is shown.

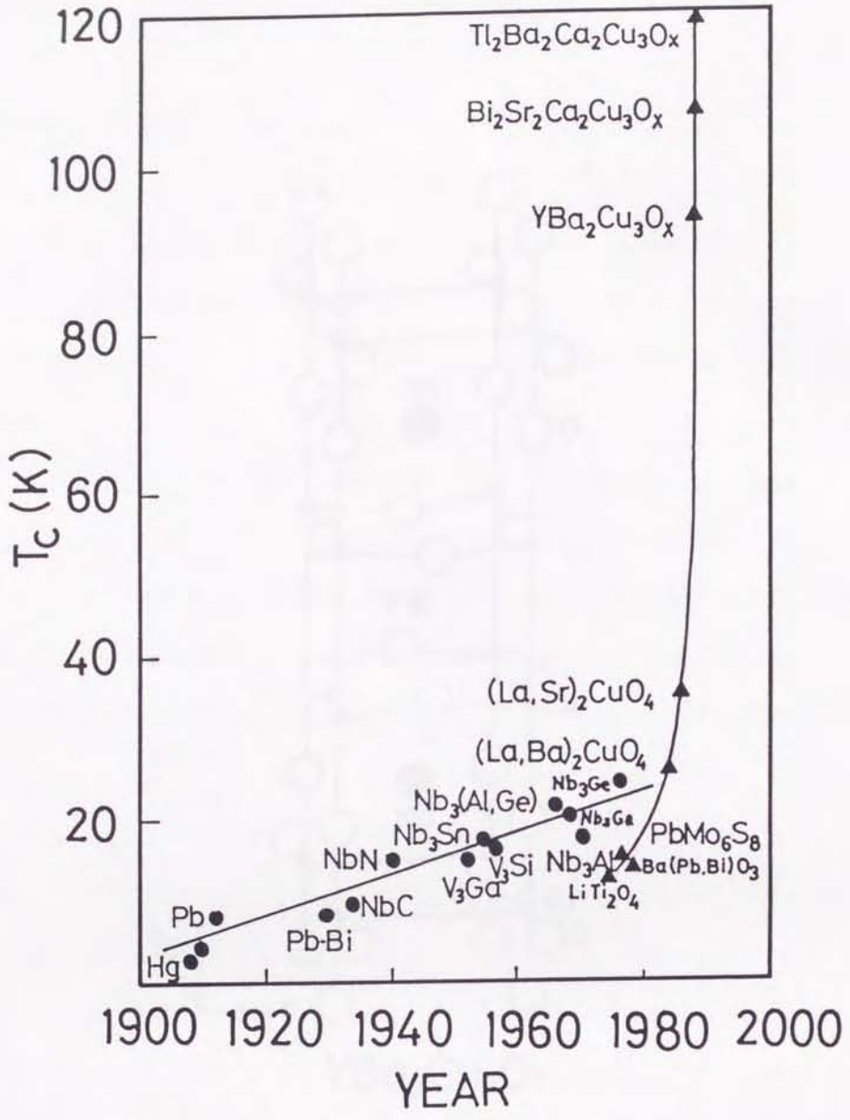

Fig. 1.4. History of the discovery of superconductors (● metals and metallic compounds, ▲ oxides and sulphides).

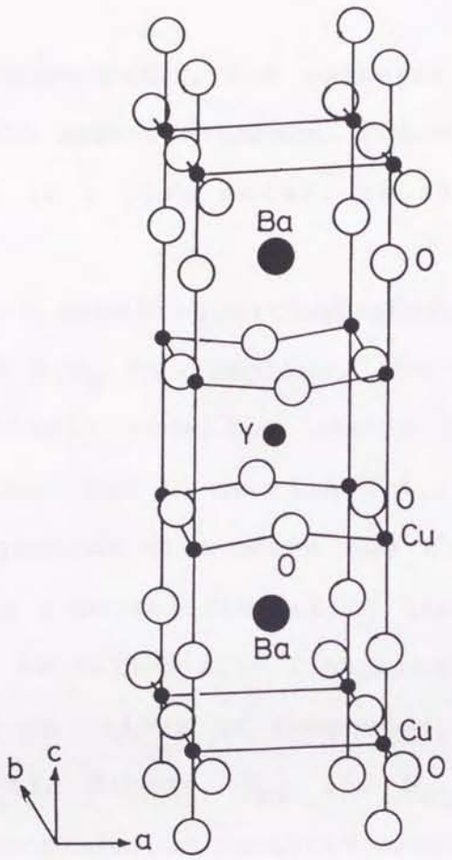

Fig. 1.5. Crystal structure of high-T_c superconductor $YBa_2Cu_3O_x$ (some of the O atoms in $YBa_2Cu_3O_7$ are deficient).

1.3. Properties of type II superconductors

1.3.1. Magnetic properties

In a superconductor, the magnetic property is as important as the zero resistance. The magnetic behaviour quite differs in a pure metal, an alloy or an oxide compound.

For a pure metal superconductor, when external magnetic field $H<H_c$ is applied, the magnetic flux is expelled completely from the inside of the superconductor (as described in section 1.1.). When H exceeds H_c, the diamagnetism disappears and the superconductor transforms into a normal conducting state. This kind of superconductor is called type I superconductor.

Meanwhile in alloys or compounds, there are two critical magnetic fields, H_{c1} and H_{c2}. When $H<H_{c1}$ or $H>H_{c2}$, the superconductor exhibits magnetic behaviour as same as that in a type I superconductor. However, for $H_{c1}<H<H_{c2}$, flux gradually penetrates into the sample, but even at the thermodynamic equilibrium this flux is smaller than that in the normal state. A new state appears in which a lattice of quantized flux-enclosing supercurrent vortices is formed: this state is commonly called the "mixed state".

A schematic variation of the magnetization versus the field H and the flux lattice in a type II

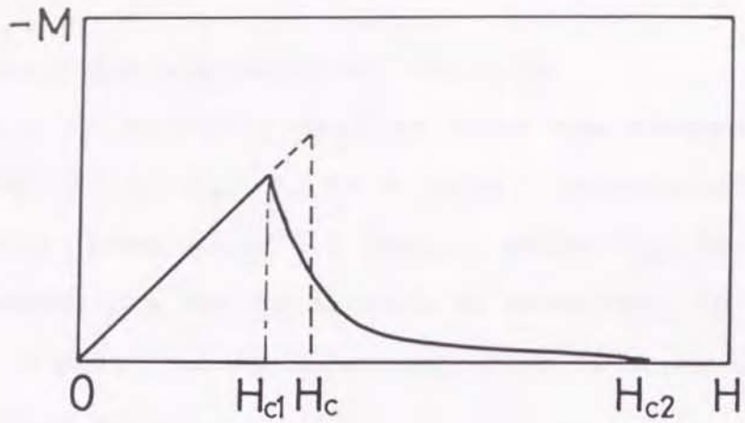

a)

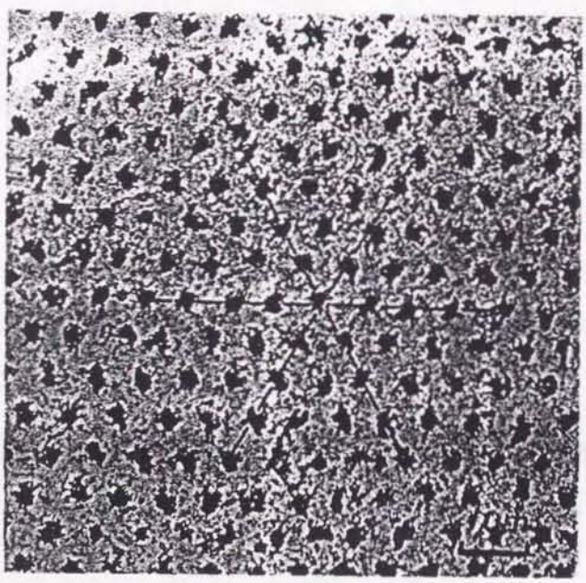

b)

Fig. 1.6. a) Schematic variation of the magnetization versus the field H in a type II superconuctor;

b) An illustration of the "mixed state" in a type II superconductor: normal regions of small radius (quantized fluxes) are embedded in a superconducting matrix (by Essmann and Trauble[7]).

superconductor are shown in Fig. 1.6.

H_{c1} is normally smaller than the thermodynamic critical field H_c. H_c in a type I superconductor is generally lower than 0.1 Tesla, while H_{c2} in type II superconductors can be as high as more than 10 Tesla.[8] Hence in practical applications, type II superconductors are widely used.

1.3.2. Critical current density

As a consequence of the existence of $H_c(T)$, there is a critical current density $J_c(T)$ which drives the superconductor into the normal state. A current density $J_c(T)$ produces a magnetic field $H_c(T)$ at the surface of the superconductor.

Therefore there are three critical parameters for a superconductor, T_c, $H_c(T)$ and $J_c(T)$, each of them is correlated to other ones. Superconducting state exists only in an enclosed T-H-J space. In Fig.1.7, the situation for a type II superconductor is shown. High value of each critical parameter is necessary for practical applications: high T_c makes the cooling easy, H_{c2} implies the ability to generate high magnetic field, high J_c is necessary for the production of high field and the minimization of the superconductor magnet.

It has been described that in type II superconductors, superconductivity may exist in very

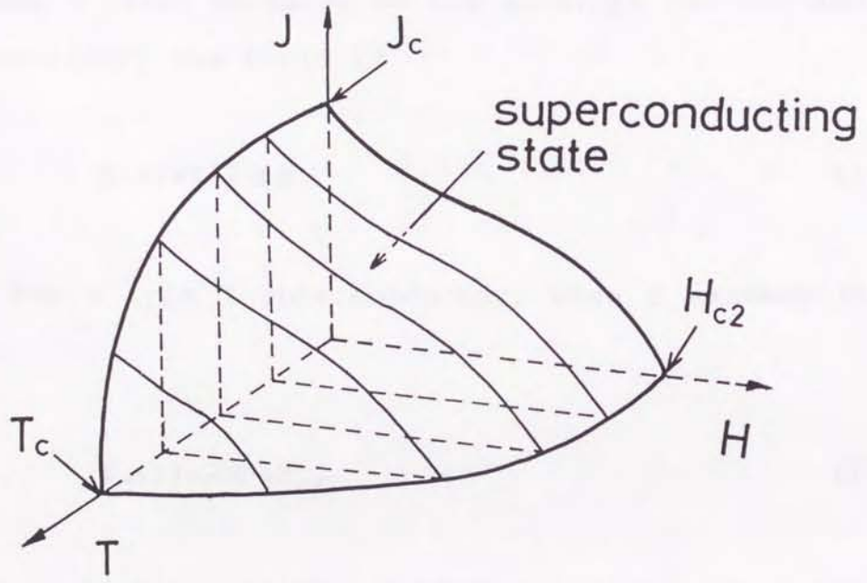

Fig. 1.7. Phase diagram of a type II superconductor (enclosed: superconducting state, outside: normal state).

high fields (H_{c2}>10 Tesla). Therefore the critical current density J_c might also be expected to be very high. Actually, for thermodynamic equilibrium this critical current density is smaller than that of a type I superconductor having the same critical field H_c.

This can be seen by calculating the theoretical current density J_c for a cylinder of radius a in which a current I flows parallel to the axis. At the surface of the cylinder, the field is

$$H(a)=I/2\pi a. \qquad (1.3)$$

For a type I superconductor, when I exceeds the value

$$I_c(I)=2\pi aH_c, \qquad (1.4)$$

where I_c is the critical current from which the critical current density J_c can be obtained, the cylinder must become a normal conductor close to the surface, and the flow of current is accompanied by heat dissipation.

For a type II superconductor, as long as $I/2\pi a<H_{c1}$, the Meissner effect is perfect and the current flows in a region close to the surface of width λ which is the penetration depth of the field. When H(a) exceeds H_{c1}, dissipation of energy occurs, and the critical current I_c(II) is given by

$$I_c(II)=2\pi aH_c. \qquad (1.5)$$

This critical current is smaller than $I_c(I)$, as $H_{c1}<H_c$.

The fact that $I_c(II)$ is given by (1.5) follows from the fact that for $H>H_{c1}$, type II superconductors are in the "mixed state" which can be roughly pictured as an array of normal regions of small radius (quantized flux) embedded in a superconducting matrix (see Fig. 1.6). As soon as I becomes greater than $I_c(II)$, fluxes appear on the surface of the cylinder. They penetrate into the cylinder and receive a Lorentz force of JxB because of the current flow. When the fluxes move, electrical field appears and heat is released.

To obtain currents higher than $I_c(II)$ it is necessary to hinder the displacement of the fluxes. Structural defects, impurities or dislocations are used to pin the flux filaments. In polycrystalline type II superconductors grain boundaries also act as pins.

Type II superconductors with pinning centres are of great technical interest because they can be used in the fabrication of superconducting magnets to produce fields of the order of 10 Tesla. Strength of the pinning can be enhanced by increasing the density of pinning centres. As long as the fluxes are pinned, it is possible for great DC current to flow without heat

dissipation. In fact, this property has been utilized widely for the conventional superconductors. For example in the widely used Nb-Ti wires, defects are intentionally created by cold working and heat treatment to act as pinning centres. The critical current density J_c can be greatly enhanced (as shown in Fig. 1.8).

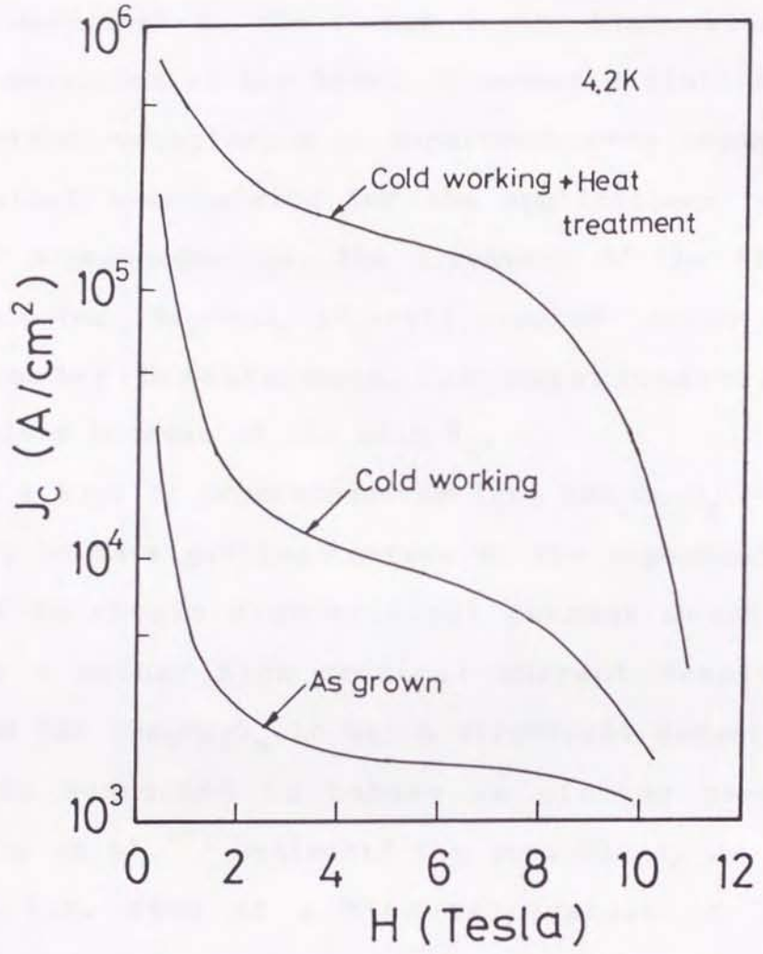

Fig. 1.8. Effect of increasing the density of pinning centres by cold working and heat treatment in Nb-Ti (by H. Takei[9]).

1.4. Critical current density in high-T_c superconductor $YBa_2Cu_3O_x$

As described in the former texts, high critical current densities at the level of magnetic field needed for specific operation, e.g. superconducting magnet, is an important prerequisite for the applications of all kinds of superconductors. The discovery of the high-T_c superconductor $YBa_2Cu_3O_x$ ($T_c \doteq 90K$) created hopes for a much broader breakthrough for superconductivity applications because of its high T_c.

For a type II superconductor like $YBa_2Cu_3O_x$, it is necessary to have pinning centres in the superconductor in order to obtain high critical current densities. Actually a rather high critical current density is predicted for $YBa_2Cu_3O_x$ in which structural defects and twins are suspected to behave as pinning centres. Matsushita et al.[10] estimated the possible J_c as shown in Fig. 1.9. Even at a high temperature of 77 K, $YBa_2Cu_3O_x$ can compete with the conventional low T_c superconductor Nb-Ti. As a matter of fact, critical current densities as high as 10^6 A/cm^2 at 77 K have been observed in single crystals and epitaxially grown thin films.[11,12]

In practical applications such as superconducting magnets, bulk materials must be used. However, the critical current densities in $YBa_2Cu_3O_x$ bulk ceramics

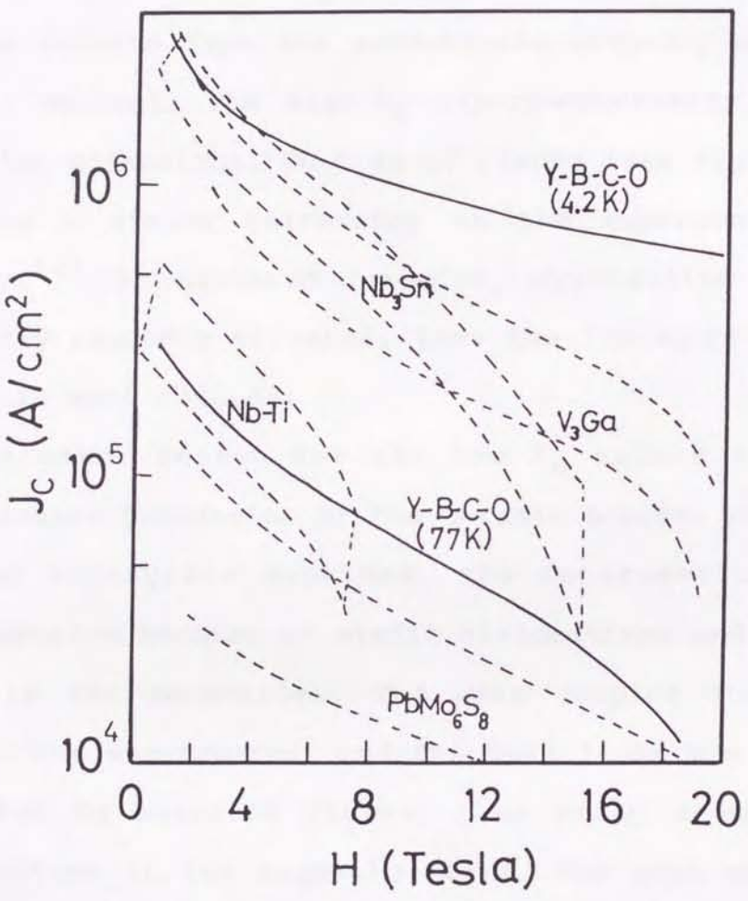

Fig. 1.9. Theoretically obtainable critical current densities for $YBa_2Cu_3O_x$ estimated from the pinning theory by T. Matsushita et al.[10] (areas surrounded by the broken lines express the obtainable values at 4.2 K for some traditional low-T_c superconductors .

are very low, having a magnitude of $\sim 10^2 A/cm^2$ at 77 K without external field.[13] This is far from the level obtained in the conventional superconducting materials in use. Two dominating reasons are known to be responsible for the low J_cs.

One results from the anisotropic property of the critical current. The high-T_c superconductivity occurs in the two-dimensional Cu-O (a-b) planes (see Fig. 1.5), producing a strong anisotropy in the superconducting property.[14] In sintered ceramics, crystalline grains are nearly randomly oriented, thus the transport supercurrent is much reduced.

The other reason for the low J_c exists in the intergranular boundaries of the ceramic sample. Compared with the intragrain sections, the intersections are weakly coupled because of misfit dislocations and second phases in the boundaries. The weak coupled junctions obstruct the supercurrent and the weak links are easily penetrated by magnetic fluxes, thus bring a quick J_c deterioration in the magnetic field. The weak coupling is related to the fundamental property of the high-T_c superconductors.

In section 1.1, it is described that the superconductivity occurs when electrons (or holes) are coupled to form electron (or hole) pairs. The range of the coupling is called the coherence length as denoted by ξ. The coherence length within which the

superconducting coupling can occur, is only several nm in $YBa_2Cu_3O_x$ or other high-T_c superconductors.[15] This is smaller than the weak link range (~0.1 μm). While for conventional low-T_c superconductors the coherence lengths have the magnitude of 1 μm. Because of the long coherence length, the grain boundaries in polycrystalline Nb_3Sn and V_3Ga behave as pinning centres rather than obstruct the supercurrent.

In wires of $YBa_2Cu_3O_x$, although the ceramic particles are close packed with a very high density as the result of the wiring process, poor J_c characteristics are exhibited (Fig. 1.10). Especially the deterioration in external fields at 77 K is undesirable.

Some efforts have been made to improve the low critical current density by enhancing the grain orientation and the packing density. Farrell et al. improved the c-axis orientation by the use of a "field-inducing" method.[17] Grader et al. reported a superficial J_c of ~3000 A/cm^2 (77K, zero field) in a hot pressed sample.[18] It should be also mentioned that recently a method of melting growth was developed by Jin et al. (J_c=17000 A/cm^2 at 77 K, zero field)[19], and modified by Murakami et al. (J_c=35000 A/cm^2 at 77 K, 1T).[20] Large crystals as large as 10 mm are grown with the high-temperature melting. Reduced granularity is reported to be the origin of the much improved J_cs.

In summary, the situation concerning the critical

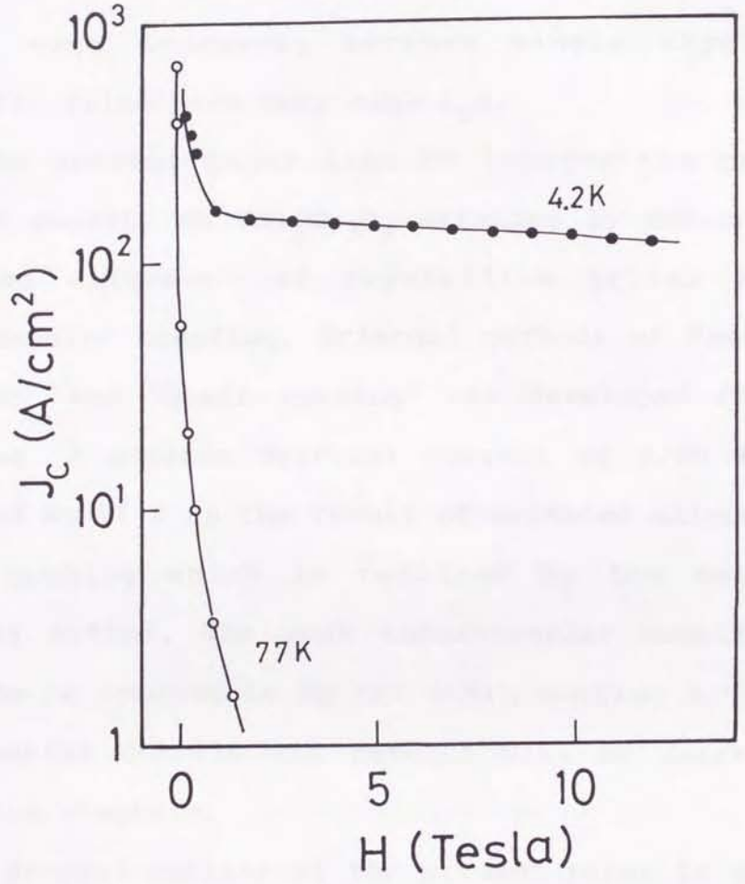

Fig. 1.10. Critical current densities in a $YBa_2Cu_3O_x$ wire (by Y. Yamada[16]).

current density in $YBa_2Cu_3O_x$ ceramics is still far from satisfying. Beside many irreplaceable merits, the ceramic materials are easy to manufacture at very low costs. However, high critical current densities would be available if the poor orientation and weak links of the grains were improved, because single crystals or epitaxial films have very high J_cs.

The present paper aims to improve the critical current density in $YBa_2Cu_3O_x$ ceramics by enhancing the oriented alignment of crystalline grains and the intergranular coupling. Original methods of "mechanical aligning" and "grain coating" are developed for these purposes. A maximum critical current of 4200 A/cm^2 is obtained at 77 K as the result of oriented alignment and close packing which is realized by the mechanical aligning method. The weak intergranular coupling also seems to be improvable by the grain coating method. The experimental details and results will be described in following chapters.

A general outline of the present paper is given as follows.

1.5. Outline of the present paper

The present paper consists of 6 chapters:

Chapter 1 gives a brief introduction to superconductivity and high-T_c superconductors. The actual state-of-the-art and the remaining problems for practical applications of the high-T_c superconductors are reviewed from the engineering point of view.

Chapter 2 presents a "mechanical aligning" method for preparation of highly oriented $YBa_2Cu_3O_x$ ceramics in order to improve the J_c characteristics. Experimental results concerning the critical current density are reported.

In Chapter 3, effect of the "mechanical aligning" on the microstructures is clarified by a combined study of experiments and theoretical analyses. The enhancement in J_c is explained by analyzing the correlation between J_c and the extent of dense packing.

In Chapter 4, An irreversible property of the critical current density is discussed. A comparison study shows that the weak coupling between oriented blocks is responsible for this irreversibility and hinders the realization of higher critical current densities.

In Chapter 5, a "grain coating" method is presented to improve the intergranular coupling. Promising results are observed.

Finally, in Chapter 6, important results as well as remaining problems are summarized.

2. IMPROVEMENT OF CRITICAL CURRENT DENSITY IN POLYCRYSTALLINE $YBa_2Cu_3O_x$ CERAMICS

2.1. Introduction

Since the discovery of high-T_c oxide superconductor,[4,6] much research has been made on the ceramic materials. Due to these efforts, it became clear that the superconducting property could be affected by the preparation process of the ceramic material. In particular, the critical current density J_c varies extensively according to different preparations. However, J_c value of samples prepared by conventional techniques remains low (e.g. not more than a few hundred A/cm^2 (77K) at zero field for $YBa_2Cu_3O_x$ [13]). Nevertheless, this low J_c could be improved if high orientation and close packing of crystalline grains were obtained, because single crystals grown from melt have very high J_cs.[11]

We have tried to improve J_c by developing a "mechanical aligning" method which involves "large crystallite growth" and "vibrational alignment of crystalline grains under a fixed boundary".[21,22,23] Large crystallites are employed to take advantage of their anisotropic morphology on cleavage and the vibration is intended to align these crystals to achieve dense and ordered packing. The anisotropic morphology is

strong in the large crystallites in which crystals grow preferentially in the a-b planes, therefore c-axis oriented alignment of the grains will be obtained by uniaxial pressing. An intermediate vibration before the pressing promotes the inclined c-axis orientation.

In the following text, preparation of highly oriented $YBa_2Cu_3O_x$ ceramics by this technique will be described. Results of J_c measurement will be also reported.

2.2. Experimental details

Powders of Y_2O_3 (purity:99.9%), $BaCO_3$ (99%), and CuO(95%) were mixed by molar ratio 1:2:3, calcined at 900 °C for 12 hours, pelletized and heated again at 900 °C for 6 hours. All heat treatments here and below were carried out in oxygen gas flow (0.3l/min). The pellets were ground, repelletized, heated at 1000 °C for 60 hours, and finally ground into individual crystalline grains. A major part of these ground grains were long rectangular plates, with grain size ranging from ~10μm up to ~100 μm. One of the large grains is shown in Fig. 2.1. Small grains were excluded by a 635-mesh sieve since we appreciate the large grains for their anisotropic morphology. Such grains were set into a rectangular cell with fixed boundaries to be aligned by a mechanical vibration, then pressed (5 ton/cm^2).

Process of the vibrational aligning is illustrated in Fig. 2.2. Here the boundaries were made with soft paper sheets, and the vibration in this experiment was produced simply by a RC oscillator and a speaker. After the vibrational treatment the boundaries were cut away, and samples with dimensions of ~0.3x1x8 mm^3 were obtained. Thereafter a resintering at 950 °C for 5 hours was practiced.

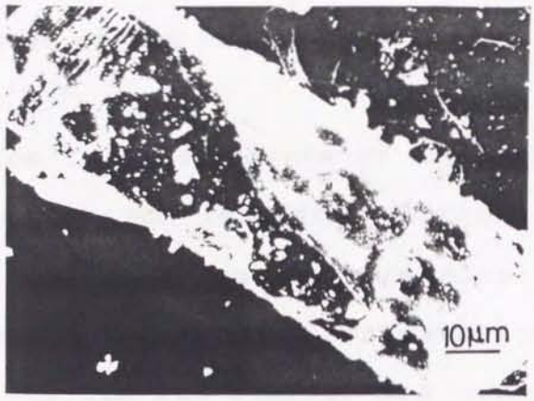

Fig. 2.1. A large crystalline grain grown at 1000 °C.

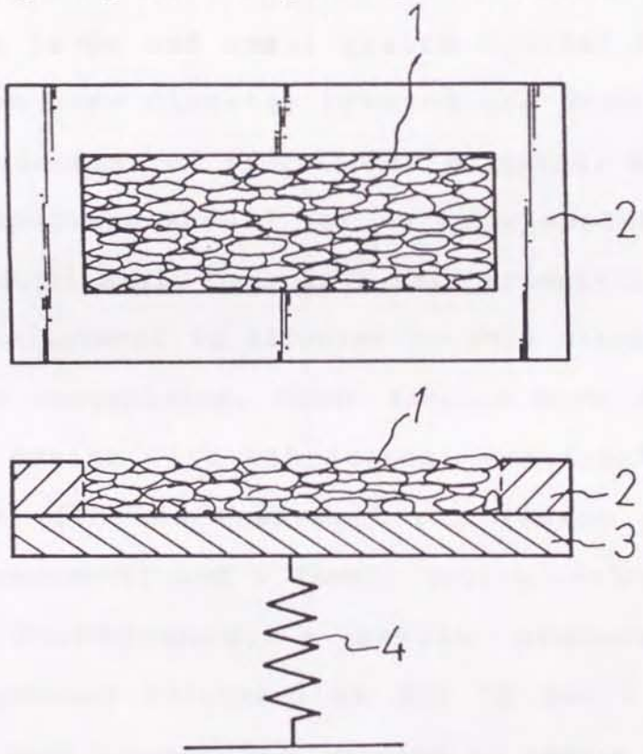

Fig. 2.2. Illustration of the vibrational aligning process (1: grains, 2: cell, 3. steel block and 4: vibrator).

2.3. Results and discussion

2.3.1. Assessment of the present method

In addition to measurements of T_c and J_c, X-ray reflection spectra, SEM (scanning electron microscope) microstructure and bulk density were also investigated for assessment of the crystal orientation and grain alignment. To confirm and clarify the expected effects of the present process, the excluded small grains were also treated by the same process for comparison. Besides, both large and small grains divided by the 635-mesh sieve were directly pressed and resintered without the treatment of vibrational aligning. Results from this comparison should let us know whether the large grains excel small ones in c-axis orientation and whether grain alignment is affected by this vibrational treatment. For convenience, these samples were denoted as **LV** (large grains with vibrational treatment), **SV** (small grains with the treatment), **L** (large grains without the treatment) and **S** (small grains without the treatment). Furthermore, a sample prepared by conventional process (sintered at 950 °C for 5 hours after several heat treatments), denoted as sample **A**, was also investigated for comparison.

X-ray (CuKα,30KV) reflection is conducted on the uniaxially pressed surface of the sample, which is

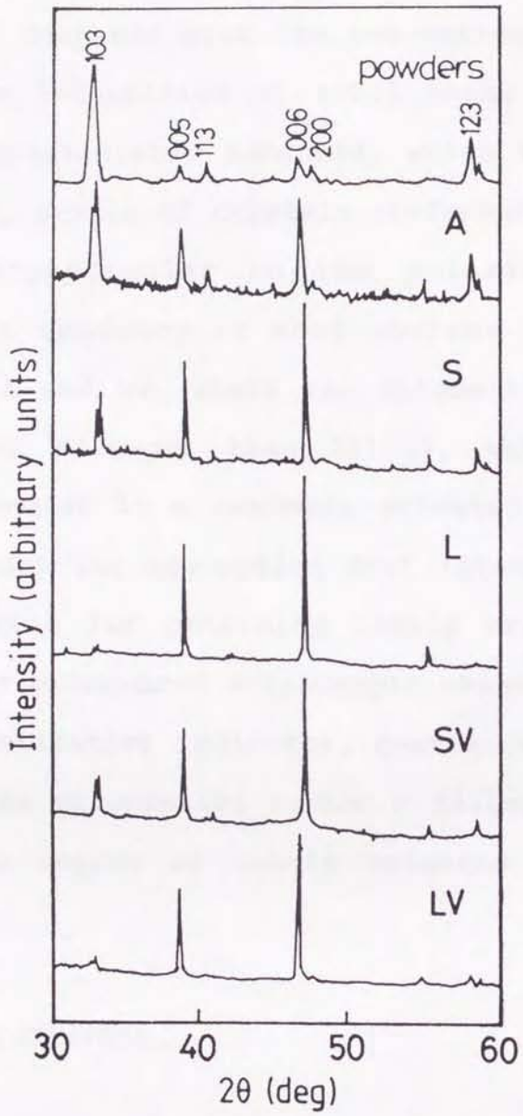

Fig. 2.3. X-ray reflection spectra of samples **A**, **S**, **L**, **SV** and **LV** as well as fine powders.

perpendicular to the c-axis in an oriented sample. In Fig. 2.3, the intensity (arb. units) patterns are demonstrated. Compared with the conventionally sintered sample **A**, the intensities of (001) peaks of the other samples are considerably enhanced, which means that in these samples, c-axis of crystals preferentially lies in direction perpendicular to the uniaxially pressed surface. This tendency is most obvious in the large grain sample **L** and **LV**, where the intensity I(001)s are generally much stronger than I(103), which otherwise would be strongest in a randomly oriented sample. This seems to support our assumption that larger crystallite is more suitable for obtaining highly oriented sample because of its pronounced anisotropic shape.

As a quantitative indicator, c-axis orientation is estimated by an orientation factor P defined by K. Chen et al.[24] The degree of c-axis oriented alignment is expressed as

$$P=(1-T)\times 100\%. \qquad (2.1)$$

Here T is the relative intensity of non-001 reflection compared to an unoriented sample which could be written as

$$T=[1-\Sigma I(001)/\Sigma I(hkl)]/[1-\Sigma I_R(001)/\Sigma I_R(hkl)] \qquad (2.2)$$

where I_R represents the intensity of the randomly oriented sample.

Limiting 2ϑ to 30-60 degrees, and regarding the powders (crushed from **A**) as an unoriented sample for reference, P was found to be 24%, 51%, 83%, 59% and 81% respectively for samples **A, S, L, SV, LV.**

As a more reliable alternative to value the degree of orientation, a different method of X-ray reflection was also used. The reflection was conducted similarly on the uniaxially pressed surface of the sample. However, in this experiment, the reflection was measured at continuously varied incident angle ϑs while 2ϑ was locked at the Bragg diffraction angle of the (006) peak. As the result a sharp distribution of the reflection versus the incident angle ϑ would imply a c-axis oriented alignment in the ceramic sample. Therefore, the orientation degree can be judged by the half width 2γ of the distribution. Distributions of sample **LV**, sample **A**, and powders (slightly pressed) are shown in Fig. 2.4. The half width 2γ was found to be 4^{o},12^{o} and 18^{o} respectively for LV, A and the pressed powders, approving the valuation by orientation factor P.

An interesting fact was also found by us. The distribution of I versus ϑ for the oriented sample **LV** could be well fitted by a Lorentz function expressed as

$$I(\vartheta)=\gamma^2/[(\vartheta-\vartheta_0)^2+\gamma^2]. \qquad (2.3)$$

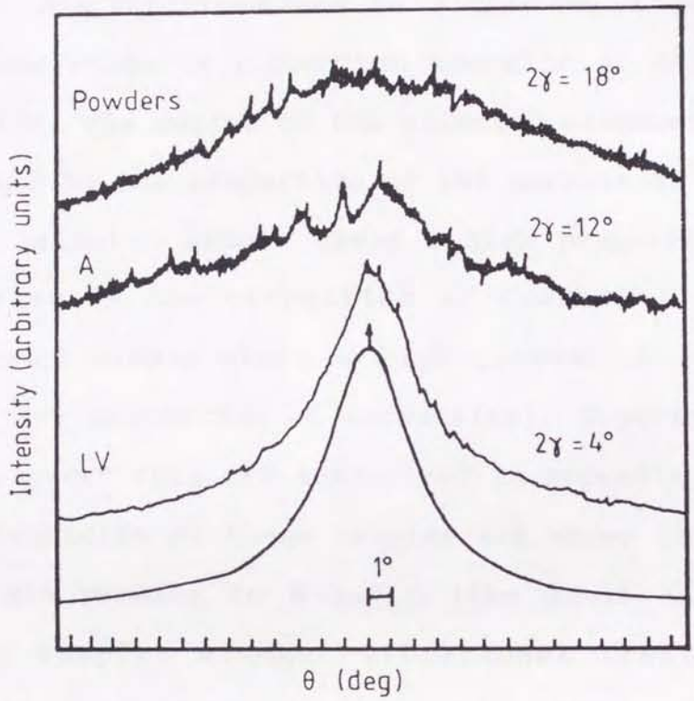

Fig. 2.4. Distributions of the X-ray reflection versus ϑ with 2ϑ locked at 006 peak (top: poorly oriented powders, middle: the conventionally prepared sample A, bottom: the mechanically aligned sample **LV.**) and a calculated Lorentz function $I(\vartheta)=\gamma^2/((\vartheta-\vartheta_0)^2+\gamma^2)$ with $2\gamma=4^o$ (the smooth line).

The function is well known in mechanics, where it corresponds to the resonance curve of an oscillator in harmonic oscillation. On the other hand, for the poorly oriented samples the fitting was not so good. As a matter of fact, we have discovered that all of the reflection distributions can be fitted to a pseudo-Voigt function which is a combined function of Gaussian and Lorentzian. The degree of the oriented alignment can be also judged by the proportion of the Lorentzian part, i.e. a well oriented sample gives a high proportion of the Lorentzian (a low proportion of Gaussian) and a poorly oriented sample shows a high proportion of the Gaussian (a low proportion of Lorentzian). Experimental results to support this are summarized in Appendix.

Microstructures of these samples are shown in Fig. 2.5. The grain packing in **S** and **L** (the small and the large grain samples without vibrational treatment) resembles that in A (the conventionally prepared sample). However, in **SV** and **LV** the packing is considerably denser than that in **S**, **L** or **A**. This is apparently an effect of the "vibrational alignment". Because of the mechanical vibration, the grains seem to be closely packed. Beside the packing density, the degree of oriented alignment is also important in discussing the packing. In sample **LV**, dense packing as well as oriented alignment has been reached. Meanwhile for sample SV the oriented alignment of grains are not

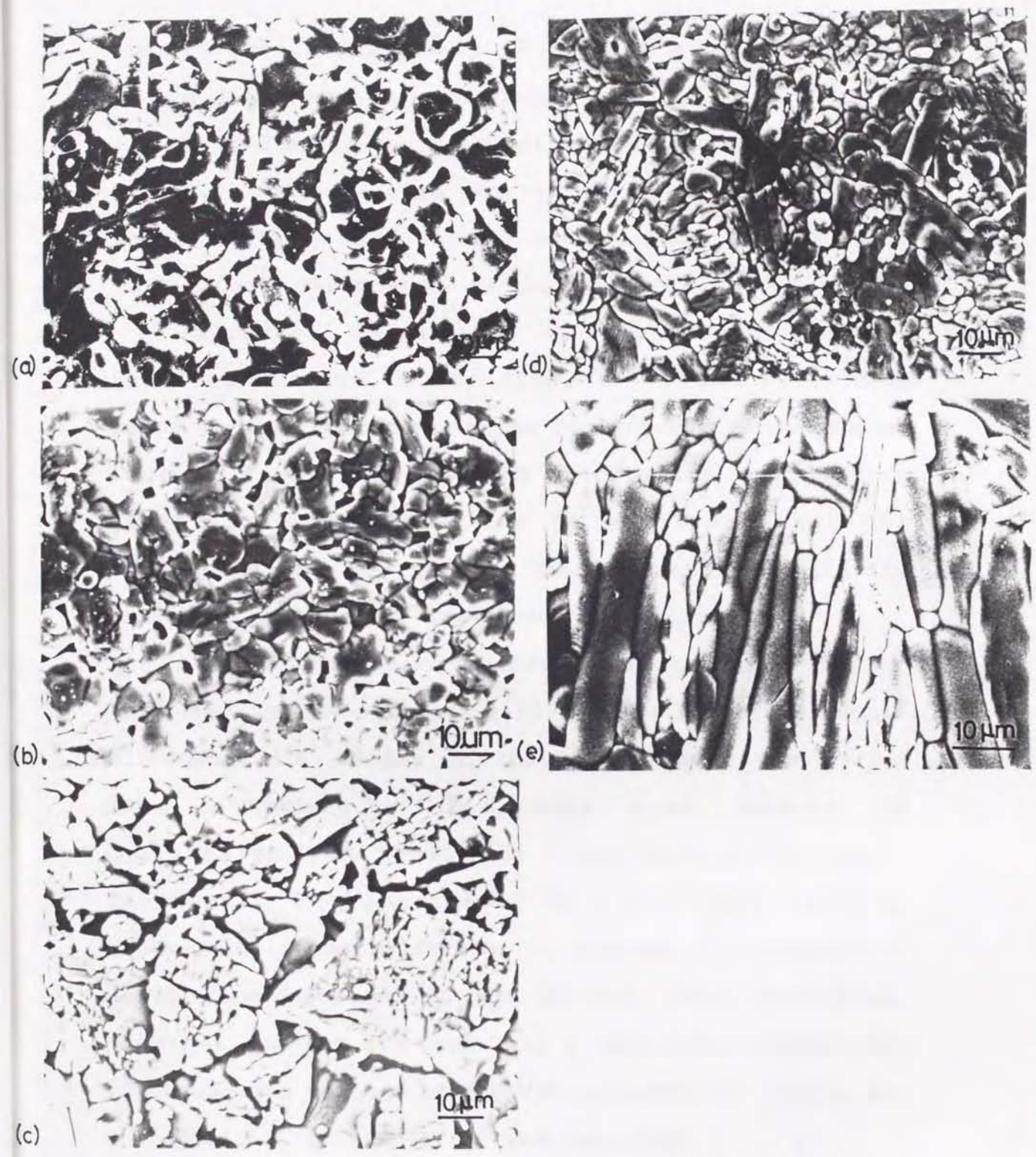

Fig. 2.5. Surface SEM images of (a)**A**, (b)**S**, (c)**L**, (d)**SV** and (e)**LV**.

observed. This difference is clearly a natural result of the difference in morphology.

Bulk density was measured to be approximately 5.2, 5.2, 5.0, 5.7, 6.0 g/cm^3 for sample **A**, **S**, **L**, **SV**, and **LV** respectively. A high density near the theoretical value (6.36 g/cm^3) was reached in the **LV** sample.

Electrical resistivity at room temperature was found to be 1.36, 0.98, 0.88, 0.60, and 0.51 $m\Omega \cdot cm$ respectively. Reduction in the resistivity is considered to be a result of enhanced orientation and packing density. Therefore it can be concluded that the orientation degree, packing density, and conductivity have been enhanced by the present technique.

The measurement of critical current density J_c was performed by use of a standard 4-probe method in liquid nitrogen bath. Sample in this measurement was shaped into a rectangular form, with cross section of ~0.3mmx1mm and length of ~4mm between current terminals. The electrical contacts were made by ultrasonic indium soldering. To enhance the connection, silver was deposited on the contact areas beforehand. Steady DC current was used, and J_c was determined at the point where a voltage of 1 $\mu V/cm$ appeared. In sample **LV**, a highest J_c of 4200 A/cm^2 was recorded.

The result of J_c measurement (the maximum values), together with the experimental results of orientation factor P, bulk density ρ_d, resistivity ρ_e are summarized

in Table I. All of them are consistent to show the practicality of the present process for improvement of J_c.

Table I. Critical current density J_c, orientation factor P, half-width 2γ, bulk density ρ_d and electrical resistivity ρ_e (300 K) for the conventional sample **A**, the small and the large grain sample **S**, **L**, and the vibration-processed samples **SV** and **LV**.

Sample	**A**	**S**	**L**	**SV**	**LV**
J_c (A/cm^2)	250	520	980	600	4200
P (%)	24	51	83	59	81
2γ ($^\circ$)	12	—	—	—	4
ρ_d (g/cm^3)	5.2	5.2	5.0	5.7	6.0
ρ_e ($m\Omega \cdot cm$)	1.36	0.98	0.88	0.60	0.51

2.3.2. Influence of the resintering temperature

To investigate the influence of the resintering heat treatment in the present process of **LV** sample preparation, the last heat treatment was also tried at 900 °C(48 hours), and 1000 °C(1 hour) beside the 950 °C(5 hours) treatment. J_c values were found to be 1700-2100 A/cm^2 for 900 °C samples, and 350-440 A/cm^2 for 1000 °C samples. The 900 °C heat treatment did not produce as high J_c as the 950 °C heat treatment, and J_c of the 1000 °C samples greatly deteriorated.

It has been also observed that during the J_c measurement of the 900 °C heat-treated samples, the first current cycling gives lower J_c than the following cycles (the increase is about 10%), which is considered to be a phenomenon resulting from the existence of weak intersections between aligned areas.[25)]

SEM images of the fractured cross sections of these samples, as shown in Fig. 2.6, may help to explain the result of J_c measurement. As seen from these photographs, areas of crushed fine powders (circled) can be recognized in the relatively low temperature (900 °C) treated sample. The fine powders were formed during separation of the large crystalline grains. Despite the long (48 hours) resintering, part of these powders have remained, which is undesirable because of the weak path for current flowing. This is perhaps the reason for the

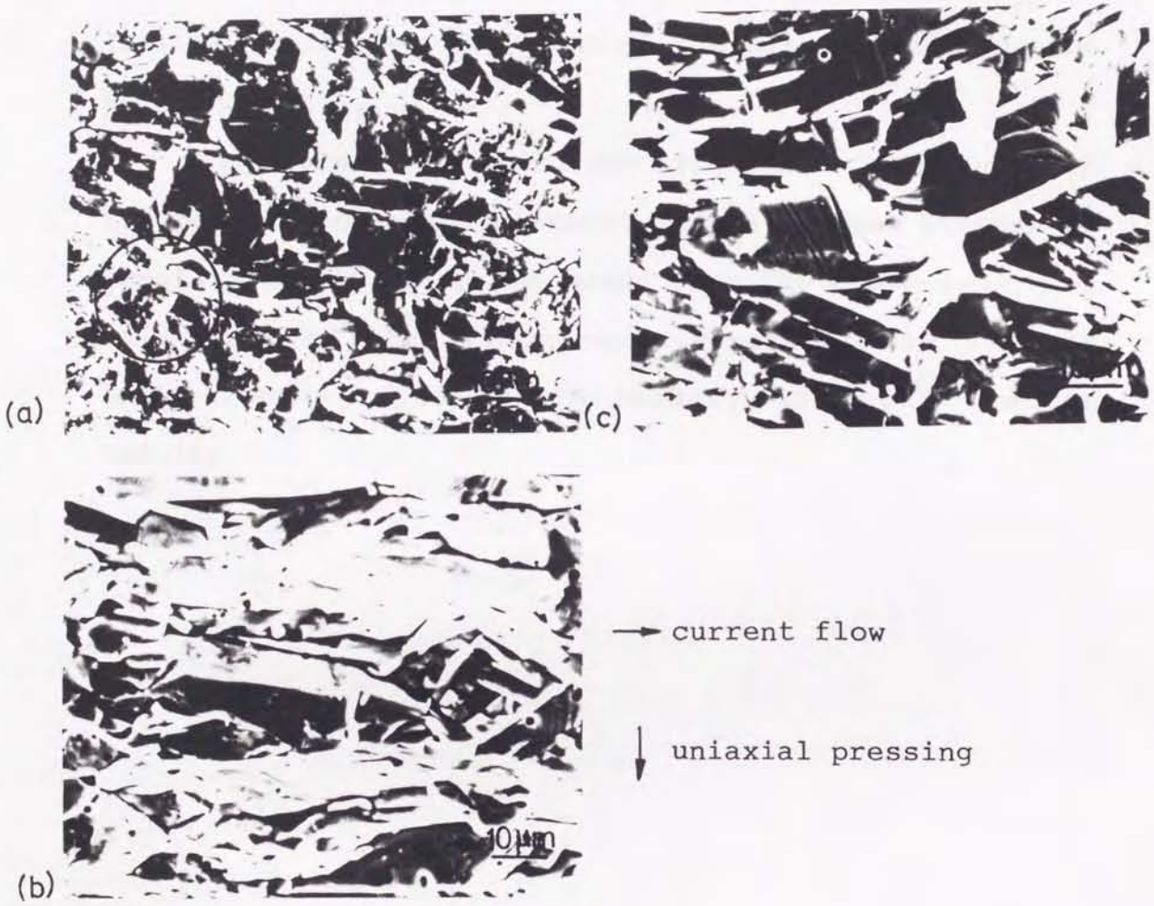

Fig. 2.6. SEM images of the fractured cross sections of samples sintered at (a)900°C, (b)950°C and (c) 1000 °C (directions of the current flow in J_c measurement and the uniaxial pressing are illustrated by the arrows).

lower J_c. On the contrast, in 1000 °C treated sample, grains seem strongly connected to each other. Nevertheless, the grains are ill-aligned due to the over-regrowth caused by the high-temperature heat treatment. This is considered to be one of the main reasons for the much reduced J_c.

Therefore, the conclusion that J_c is influenced by the resintering heat treatment in the present process of sample preparation can be drawn from the above analysis. Adjustment of the conditions (temperature as well as heat treating time) is necessary to obtain better results.

2.4. Conclusion

Highly oriented $YBa_2Cu_3O_x$ ceramic samples were prepared by a "mechanical aligning" processing technique which involved large crystallite growth and vibrational alignment of the crystalline grains. Samples prepared by the present technique were assessed by experiments of X-ray reflection, SEM, bulk density, and J_c measurement. In these samples, crystalline grains were found to be highly oriented and closely packed. A maximum J_c of 4200 A/cm^2 at 77 K, a great improvement of the conventional value (250 A/cm^2), was obtained. It was also found that J_c characteristics was influenced by the resintering conditions.

From the experimental results it was clarified that J_c is strongly related to the microstructure. In the next Chapter, a detailed study about the effect of the intermediate vibration on the microstructures will be introduced.

3. EFFECT OF INTERMEDIATE VIBRATION IN $YBa_2Cu_3O_x$ CERAMIC SAMPLES

3.1. Introduction

In Chapter 2, a considerable increment in J_c (from 250 A/cm^2 to 4200 A/cm^2 at 77 K) has been obtained with the application of the "mechanical aligning" method which involves "large crystal growth" and "vibrational alignment" of the grains.

The X-ray and SEM experiments have proved that the large crystalline grains are easier to be orientated for their anisotropic morphology and the vibrational treatment promotes the inclined c-axis orientation as well as density.

In this Chapter, further studies will be made to clarify the J_c-improving effect of the intermediate vibration.[26)]

3.2. Experimental details

Sample preparation is the same as described in 2.2. In order to investigate the effect of the intermediate vibration, uniform-sized (20-50 μm) large grains were used. The vibrational treatment was practiced at various conditions. Two parameters, frequency f and amplitude a, of the vibration movement $a\sin\omega t$ ($\omega = 2\pi f$) were varied in this process. Frequency was read from the electrical signal $V\sin\omega t$ generated by the RC oscillator and amplitude was calculated from the voltage amplitude V since the vibration amplitude a is very small. In the act of varying frequency, the amplitude was kept to be constant (1.0×10^{-7} m), and vice versa (16 kHz). Samples as prepared were resintered at 900 °C for 48 hours (the low-temperature heat treatment was used for investigation of the vibrational effect since the extent of regrowth of grains is smaller in this situation).

Critical current densities were measured in external magnetic fields perpendicular to the broad surface of the sample (parallel to the c-axis in oriented samples). The current flows in the direction of the oriented alignment.

3.3. Results and discussions

J_c of samples prepared by the intermediate vibrational process was measured in zero as well as in external magnetic fields. Results of varying frequency and amplitude are shown in Fig. 3.1 and Fig. 3.2 respectively. In each case three or more samples treated by the same vibration (same frequency and amplitude) were measured. In the measurement of J_c attention was paid to ensure that samples with cracks were excluded, thus sample dependence was greatly reduced. Samples prepared with various frequencies and amplitudes were sintered independently although the heat-treatment conditions were set to be equal. J_c was found to be relevant to the vibrational parameters. Samples treated by definite frequency and amplitude exhibited higher J_c value than other samples, implying a most effective vibrational alignment at this condition.

As further evidence to support this J_c enhancement, the extent of c-axis orientation was investigated for these samples. X-ray reflection on the uniaxially pressed surface of the sample was utilized to estimate the degree of the orientation. The "rocking method" was used for its reliability in which 2ϑ was locked at the Bragg angle of (006) peak and the incident angle ϑ was varied. A sharp distribution (small half-width 2γ) implies c-axis-oriented grain alignment in the sample.

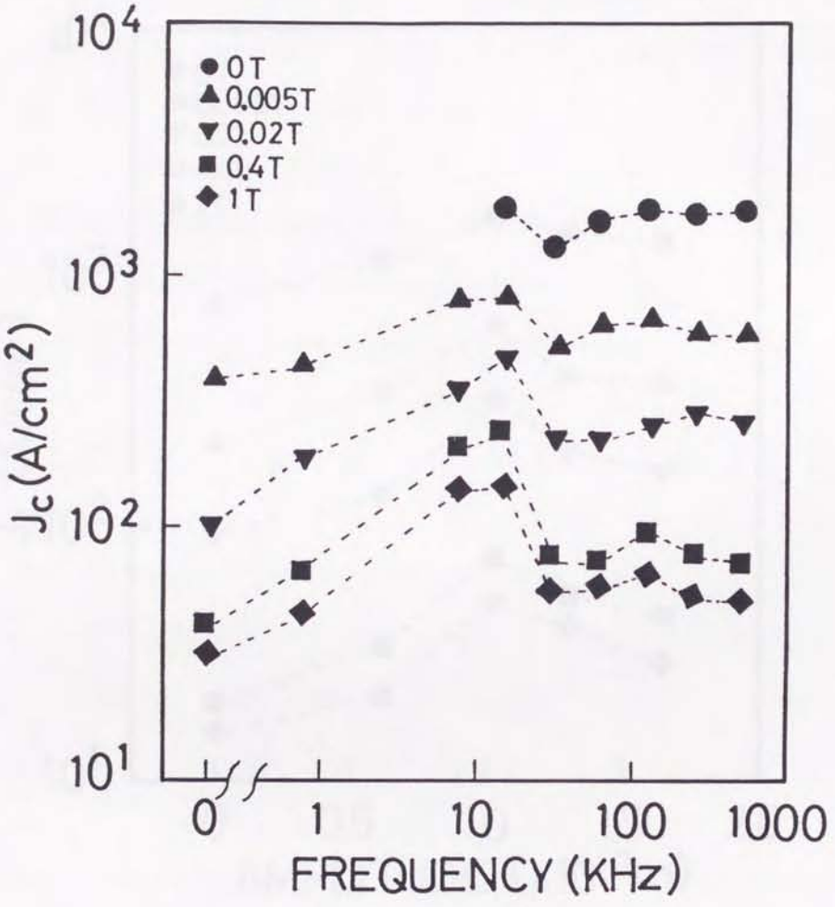

Fig. 3.1. J_c (77 K)of samples aligned by various frequencies (amplitude a of the vibration asinωt was fixed at 1.0×10^{-7} m).

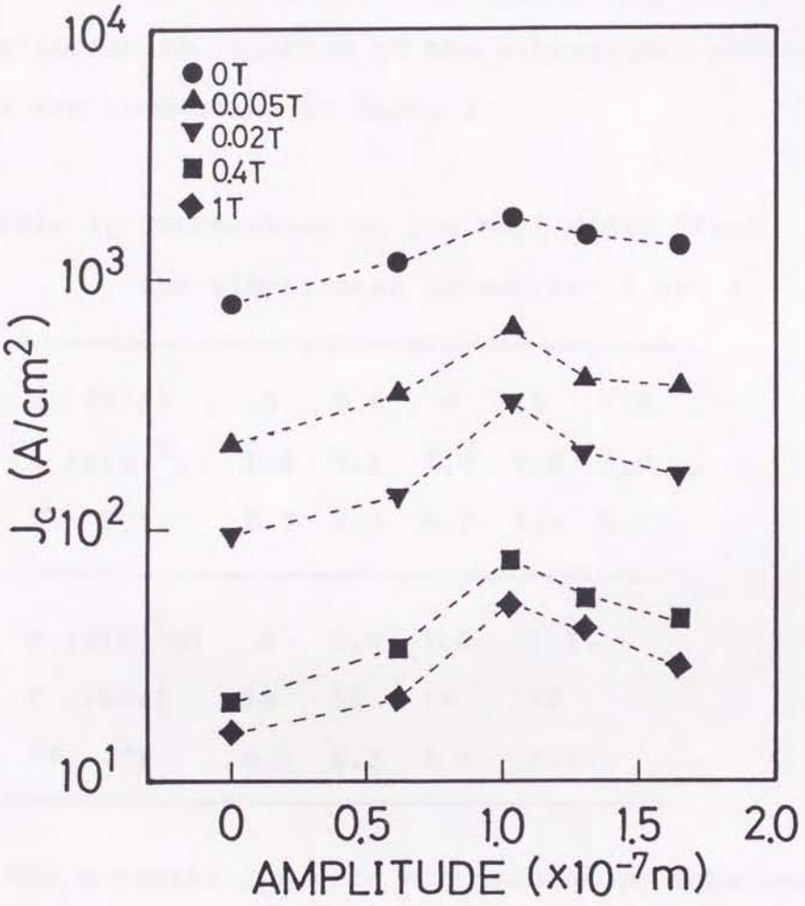

Fig. 3.2. J_c (77 K) of samples aligned by various amplitudes (frequency of the vibration was fixed at 16 kHz).

Distributions for some representative samples aligned by various frequencies and amplitudes are shown in Fig. 3.3 and Fig. 3.4. respectively.

The half width 2γs of the X-ray reflection distribution in relation to the vibrational parameters f and a are summarized in Table I.

Table I. Correlation of the half width 2γ and the vibrational parameters f and a.

f (KHz)	0	0.8	8	16	128
a ($\times 10^{-7}$m)	1.0	1.0	1.0	1.0	1.0
2γ (°)	8.3	7.3	4.7	4.6	5.1

a ($\times 10^{-7}$m)	0	0.6	1.0	1.6
f (KHz)	16	16	16	16
2γ (°)	8.5	6.3	4.8	5.2

The enhanced J_cs were accompanied by enhancement in orientation. In the sample with the highest J_c, the minimum 2γ values were also observed. This result reveals clearly the origin of the J_c enhancement.

From analyses of the X-ray experiment, it became clear that the vibrational treatment enabled the ceramic grains to align orderly, as reflected by enhancement in the c-axis orientation. An optimum vibrational condition was also suggested by the X-ray experiment as well as

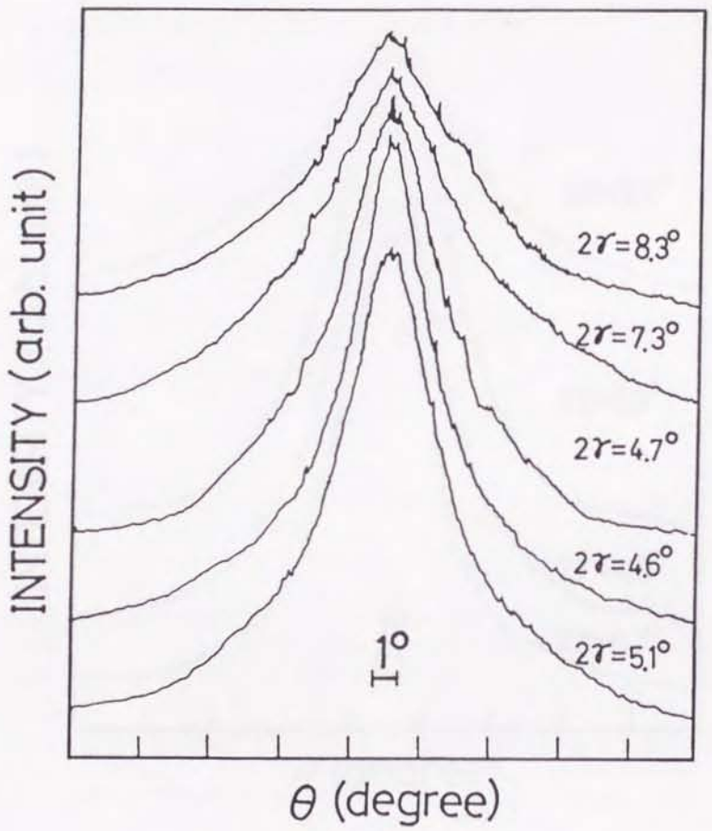

Fig. 3.3. X-ray reflection intensity versus the incident angle for samples aligned by various frequencies (from top to bottom: f=0, 0.8, 8, 16, 128 (kHz)).

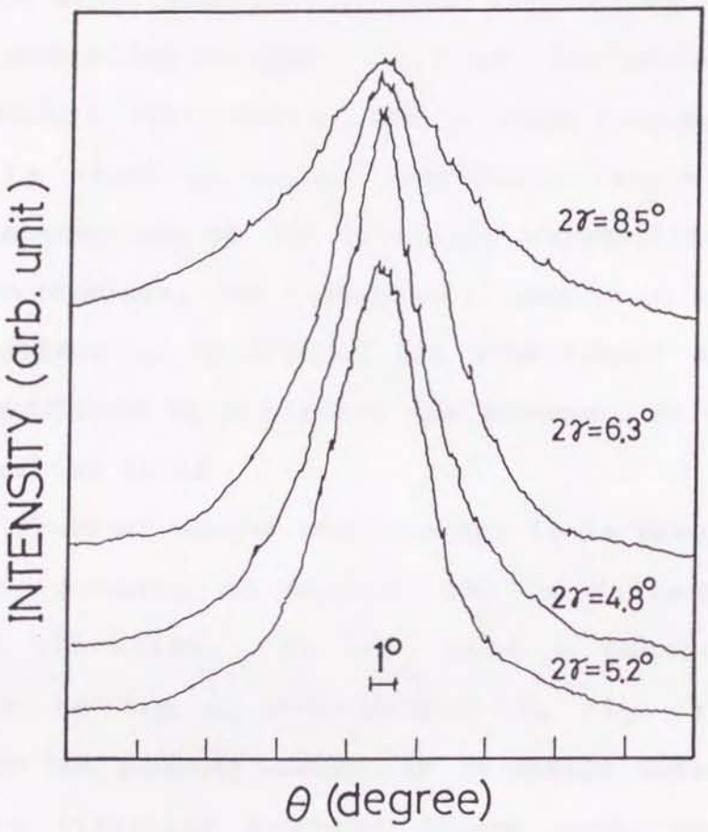

Fig. 3.4. X-ray reflection intensity versus the incident angle for samples aligned by various amplitudes (from top to bottom: a=0,0.6,1.0,1.6 ($x10^{-7}$m)).

the J_c measurement. An effort was also made to qualitatively explain the J_c enhancement. The existence of the optimum frequency is probably related to the crystallite size. Considering the limitation of the vibration-generating equipment used here (reliable range of the speaker: 20Hz-20kHz), the optimum frequency is suspected to exist in higher ultrasonic ranges where stronger interaction of the vibrating crystallites may appear. Nevertheless, the experimental result on varying amplitude allows us to discuss the vibrational effect, which is performed by analyzing the movement of grains in the vibration field.

In the field of powder engineering, it is known that the packing density of powders can be raised by a mechanical vibration. We will give a theoretical explanation to the J_c enhancement in Fig. 3.2 by referring to the packing theory. It is easily understood that if the vibration produces denser grain packing, then the critical current density will be enhanced. The maximum J_c must be obtained with the same optimum condition of vibration which produces the highest packing.

In the former passages, we have concluded that the J_c enhancement results from the improved orientation. As a matter of fact, the packing factor and the orientation degree are considered to be representative of each other. A highly oriented alignment of the crystalline

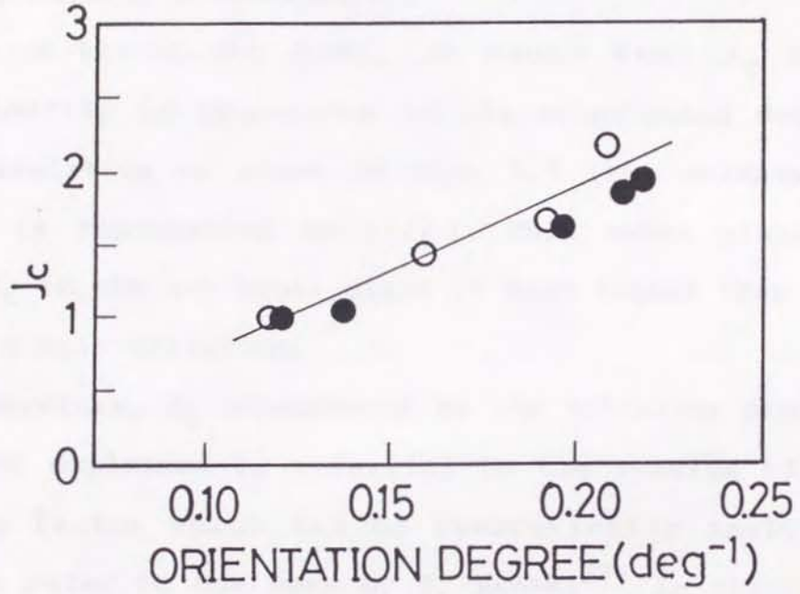

Fig.3.5. Correlation of the critical current J_c (unified by J_c of the non-vibration sample) and the orientation degree (circle: samples aligned by various amplitudes, dot: samples aligned by various frequencies).

grains will produce a dense packing in result. This can be understood by viewing the SEM image of the fractured cross section of the oriented sample (a or b in Fig. 2.6). The parallel alignment reduces the dangled inter-crossing spaces between the crystallites, raising the packing density effectively.

From the X-ray data, we found that J_c was approximately in proportion to the orientation degree. The correlation is shown in Fig. 3.5 (the orientation degree is represented by $1/2\gamma$). This seems plausible since J_c in the a-b basal plane is much higher than that in the c-axis direction.

Therefore, J_c enhancement by the vibration process could be explained by referring to the results of the packing factor which can be theoretically analyzed. Here we refer to the work by T. Tanaka[27] in which the behavior of powders in a vibration field has been analyzed.

First, let us consider the behavior of a single grain in the vibration field $a\sin\omega t$ as illustrated in Fig. 3.6.

The plate vibrates in Y direction which can be expressed as

$$Y=a\sin\omega t=a\sin 2\pi ft, \qquad (3.1)$$

where a is the amplitude and f is the frequency.

Let the movement of the grain be expressed in xy plane. Then

$$md^2y/dt^2=N-mg, \tag{3.2}$$

where N is the force received from the plate and mg is the weight of the grain.

When the grain move together with the plate, y must be equal to Y. From (3.1) and (3.2) N is derived to be

$$N=m(g-a\omega^2\sin\omega t). \tag{3.3}$$

Because $N>0$, hence

$$\sin\omega t<g/a\omega^2=1/G, \tag{3.4}$$

G is called the vibration intensity. If $G<1$, then the grain always moves together with the plate.

In (3.3), at the moment when N=0, the grain will leave the plate, Thus

$$\sin\omega t_0=1/G$$
$$\omega t_0=\sin^{-1}(1/G), \tag{3.5}$$

where t_0 is the moment at which the grain leaves the plate.

The initial speed of the grain at t_0 equals that of

the plate ($dY/dt=a\omega\cos\omega t_0$), and the location is $a\sin\omega t_0$. Hence the movement can be expressed as

$$y=a\omega(\cos\omega t_0)(t-t_0)-1/2g(t-t_0)^2+a\sin\omega t_0$$
$$=g/\omega^2[1+\omega(t-t_0)\sqrt{G^2-1}-1/2\,\omega^2(t-t_0)^2] \qquad (3.6)$$

Let the next moment at which the grain falls to the plate be t_1, then $y_{t=t1}=Y_{t=t1}$. Substitute this relation to (3.1) and (3.6), time t_1 and the speed dy/dt can be obtained.

Summarize these results, we have

$$\omega t_0=\sin^{-1}(1/G)$$
$$\omega t_1=\omega t_0+(\sqrt{G^2+1-2G\sin\omega t_1}-\sqrt{G^2-1}). \qquad (3.7)$$

In the case of many grains in a container, the movement of the grains can not be described by this simple analysis. Nevertheless the fundamental results may be used.

When the grains fall to the plate, a large relative speed between the grain and the plate ($\Delta v=dy/dt_{t=t1}-dY/dt_{t=t1}$) produces a strong packing force against the grains. These grains are bounced off again and a large initial speed $v=dY/dt_{t=t0}$ should be avoided here because of the large difference of speed between the centre grains and the side grains in the container. The inside grains are in a relatively free state to move while grains close to the boundaries are unable to move at a

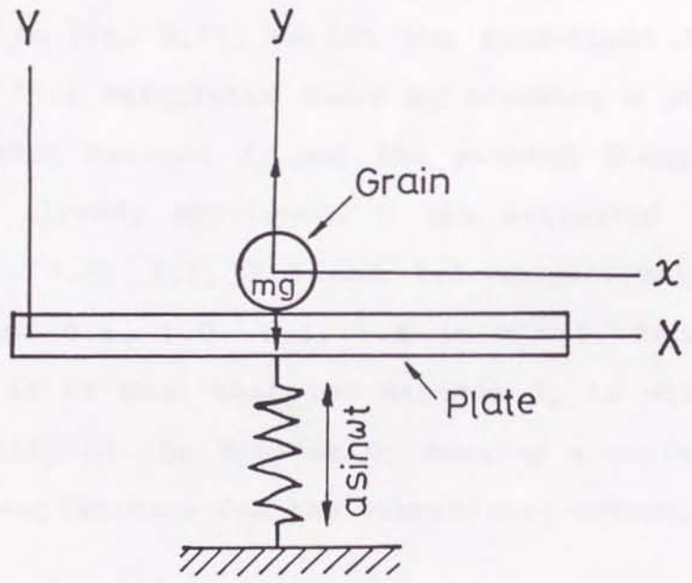

Fig. 3.6. Movement of a grain on a vibrating plate.

large relative speed as the result of friction. Therefore, the extent of the dense packing P^* could be expressed by

$$P^* = \Delta v/v = \psi_1(G)/\sqrt{G^2-1}$$

$$\psi_1(G) = \sqrt{G^2+1-2G\sin\omega t_1} + G\cos\omega t_1. \qquad (3.8)$$

Supposing that P^* corresponds in proportion to the packing density, the theoretical packing density is shown to be a function of the vibration intensity G (solid line in Fig. 3.7). We fit the zero-field J_cs of Fig. 3.3 to this calculated curve by assuming a proportional relation between J_c and the packing density P^* for reasons already mentioned. G was estimated to be approximately 1.6, 2.7, 3.4 and 4.3 respectively for amplitudes of 0.6, 1.0, 1.3, 1.6 ($\times 10^{-7}$m). From the comparison, it is seen that the maximum J_c is obtained in the vicinity of the optimum G, meaning a successful theoretical explanation for the vibrational effect.

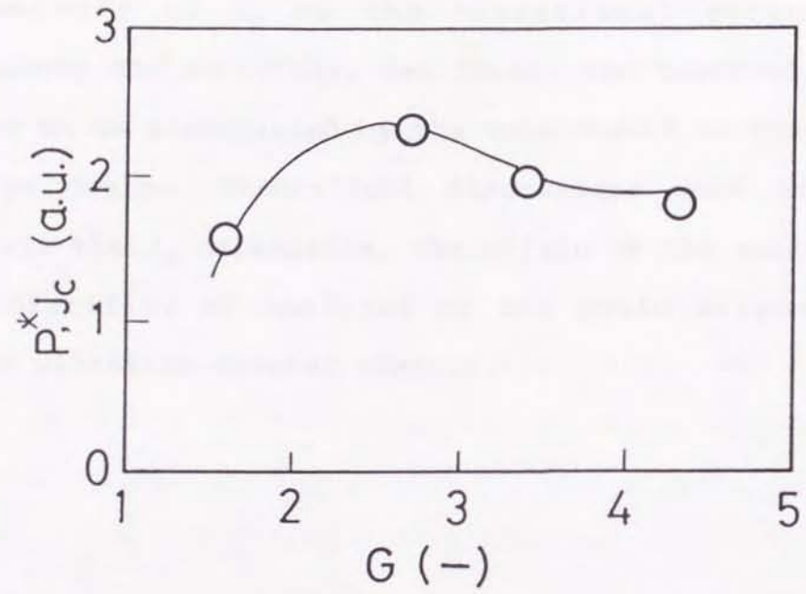

Fig. 3.7. Correlation of the critical current and the calculated packing factor (circle: J_c of the samples aligned by varied amplitudes; solid line: calculated packing density P^*. A proportional relation between J_c and P^* was supposed).

3.4. Conclusion

Transport critical current density J_c in ceramic superconductor $YBa_2Cu_3O_x$ was improved by an intermediate vibration introduced during the preparation process. Dependence of J_c on the vibrational parameters, frequency and amplitude, was found. The improved J_c was shown to be accompanied by the enhancement in the orientation degree. Theoretical discussions were tried to explain the J_c dependence. The origin of the enhanced J_c was clarified by analyses of the grain alignment in these vibration-treated samples.